Turkish Journal of Electrical Engineering & Computer Sciences

http://journals.tubitak.gov.tr/elektrik/

Research Article

Turk J Elec Eng & Comp Sci
(2017) 25: 3553 – 3568

doi:10.3906/elk-1511-232

Heuristic algorithm-based estimation of rotor resistance of an induction machine by slot parameters with experimental verification

Mehmet ÇELEBİ[1], **Murat TÖREN**[2,*]

[1]Department of Electrical and Electronics Engineering, Faculty of Engineering, Atatürk University, Erzurum, Turkey
[2]Department of Electronics and Automation, Vocational School of Technical Sciences,
Recep Tayyip Erdoğan University, Rize, Turkey

Received: 25.11.2015 • **Accepted/Published Online:** 23.04.2017 • **Final Version:** 05.10.2017

Abstract: The estimations of induction machine equivalent circuit parameters are still being widely used in the analysis and in determining the characteristics of the machine. Since the most important part of the machine is the rotor where torque is produced, the calculation of rotor resistance correctly will directly affect all other data. Almost all parameters belonging to the stator side can easily be determined through external measurements. However, due to the formulation of the rotor as a closed box, estimating rotor resistance and the rotor's slot shape by heuristic algorithms, without damaging the rotor physically, and comparing it with its actual value constitutes the first focus of this study. In this regard, rotor resistance and slot parameters are estimated through heuristic algorithms depending on the induction machine design aspects. Secondly, an improved particle swarm optimization is presented and compared with conventional PSO and genetic algorithm.

Key words: Induction machine, GA, PSO, equivalent circuit, rotor slot, optimization

1. Introduction

Online or fixed case (constant temperature, load, etc.) parameter estimation of induction machines, which has a wide commercial use today, has many industrial benefits. The correct calculation of the torque and speed and determination of equivalent circuit parameters accurately ensures the analysis of the motor in the right way. Since the fluxes on α and β axes are difficult to determine theoretically based on voltage and current in real-time applications, artificial neural networks [1], genetic algorithm (GA) [2–5], or particle swarm optimization (PSO) [6–8] and algorithm comparison (GA–PSO, GA–modified GA, PSO–modified PSO, GA–cuckoo alg., etc.) [9–14] can be used. Heuristic algorithms afford relatively easy numeric solutions for problems difficult to be solved theoretically. As induction motors are real-time systems without sensors under direct torque control (DTC), field oriented control (FOC), and vector control, aiming at determination of flux obtained through voltage and current, and determination of rotor resistance and other parameters correctly is very important [15–17]. In induction motors, sensorless control has the benefits of increasing system reliability and reducing cost [18]. Some analytical approaches also were revealed for other control algorithms in general so as to calculate stator and rotor resistance, especially rotor resistance correctly, which always exhibits variability [19–21]. Although rotor resistance is of great importance, and is one of the induction machine parameters, determination of other equivalent circuit parameters is surely required in the determination of other characteristics [22,23].

*Correspondence: murat.toren@erdogan.edu.tr

Although harmonics, skin effect, and saturation effect were not taken into consideration in the equivalent circuit, determination of these parameters has some benefits [24–26]. Other methods used to determine rotor resistance and other parameters were also presented [27–31].

Although the induction machine equivalent circuit could not yield reasonably accurate results, it is a very well-known circuit model that is still being used. The purpose of this study is to determine the slot parameters by GA, used in calculation of rotor resistance. Rotor resistance is an important parameter of equivalent circuits. Thus, calculation of rotor resistance by using geometrical design parameters will help to fill an important gap in this respect.

To obtain the slot parameters and conductive section of a closed box rotor is not easy, especially in squirrel cage induction machines. It is obvious that the processes, such as breaking the rotor to pieces and cross sectioning, will require complete renewal of the rotor. Since low power machines are cheap, breaking the rotor to pieces may not cost substantial amounts but this financial loss will be incredible for high power ones. Therefore, one of the goals of this study is to obtain a method and sight to be used in estimation of all rotor parameters without damaging the rotor.

2. Theoretical approach

The general characteristics are given in Table 1 of the task machine. In the first stage flux density and current density of the stator need to be calculated. The flux density can be determined by the following equation:

Table 1. Motor catalogue specifications.

Motor parameters		Value
lectrical	Class	IE1
	Voltage & output power	380 V & 160 kW
	Pole number	4
	Nominal torque	1029 Nm
	Starting/nominal torque	2.4
	Power factor & efficiency	0.87 & 95%
	Slip	0.01

$$B_1 = \frac{10^6.\phi.2.p}{N_1.L_i.\alpha_1.b_1} \tag{1}$$

Here B_1, φ, p, N_1, L_i, α_1, and b_1 represents flux density of stator teeth, total flux of the machine (Wb), number of pole pairs, number of stator slots, fictive stator core length (m), pole pitch factor, and stator teeth width (m) respectively. N_1, 2p, and b_1 are known values from Table 2. Fictive core length can be determined by real length of core multiplying by stack factor of lamination (stack factor is assumed as 0.95). Total flux φ of the machine can be calculated from

$$\phi = B_0\alpha_1.\tau_p.L_i \ (Wb) \tag{2}$$

B_0 and τ_p are air gap flux density (T) and stator slot pole pitch (m), respectively. In both Eqs. (1) and (2) two unknown values, air gap flux density and pole pitch factor, can be assumed as 0.75 T and 0.729, which both satisfy induction machine design limitations. On the other hand, total flux and E_1, the voltage value at the stator windings voltage drop, which is about 2% for this machine, must match with the winding number

Table 2. Measured values of 160 kW double caged induction machine.

Measured motor parameters		Value
Electrical	Winding & connection type	Whole coiled & delta
	Stator conductor total area	12.77 mm^2
	Stator current density	1.39 A/mm^2
	Parallel branches & conductor numbers for per slot	4 & 13
	Coil pitch	13
	Magnetizing current	80 A
Geometrical	Stator & rotor slot numbers	60 & 48
	Stator outer & inner diameters	500 & 325 mm
	Air gap	0.9 mm
	Stator teeth width & slot height	8.7 & 42.5 mm
	Core length	420 mm

for per phase w_1:

$$w_1 = \frac{E_1}{4.44\,.f.k_w.\phi} \tag{3}$$

and with total conductor number for per stator slot:

$$z_0 = \frac{p.m_1.w_1.a}{N_1}, \tag{4}$$

where f, k_w, m_1, and a are frequency, stator winding factor, stator phase number, and parallel branches. According to Table 2 the winding number must be 32.5 in Eq. (4) and it also must match with Eq. (3) with proper E_1 and φ values. Winding factor can be calculated simply and we can accurately measure the voltage drop (E_1) by open circuit test. Thus there are only two values that have to be accurately assumed: B_0 and α_1. To summarize this issue, the first step is to find the proper φ value that has to satisfy (2) and (5):

$$\phi = \frac{E_1.p.m_1.a}{4.44\,.f.k_w\,.\,z_0.N_1}\ (Wb) \tag{5}$$

If these two values can be achieved properly B_1 can be obtained. Thus according to these two assumptions B_1 is 1.47 T for the task machine. Then stator winding current density is calculated simply as 1.39 A/mm^2, which is based on the parameter measurement of the stator given in Table 2. The next step is to determine the induced voltage and current in each bar to find the rotor bar current as follows [32]:

$$E_{ck} = \frac{E_1}{2\,.\,w_1.\,k_w}\ (V) \tag{6}$$

$$I_{ck} = \frac{P_{mech} + P_{fric}}{N_2.\,E_{ck}.\,(1-s)}\ (A) \tag{7}$$

Here E_{ck}, I_{ck}, N_2, s, P_{mech}, and P_{fric} represent induced voltage at each rotor bar, rotor bar current, number of rotor slots, slip, and mechanical and frictional powers in W, respectively. The induced voltage and current at each rotor bar is calculated as 6.18 V and 560.17 A for this motor, some parameters of which are given in Table 1. The ring current I_{ha} is calculated through the well-known following equation [32]:

$$I_{ha} = \frac{N_2}{2.\,p.\pi}.\,I_{ck}\ (A) \tag{8}$$

After this stage, the ring width and height must be determined. Through external measurement from this point, the outer diameter of the ring that equals rotor external diameter can be determined exactly. Next, the width of the ring can be precisely measured. Although the ring height equals the rotor bar height in general, it is certain that it cannot be shorter than rotor bar height. Therefore, the ring height is assumed as equal to rotor bar height containing some margin of error. Because height of the ring can be possibly more than rotor bar height, this is a usual way to reduce the rotor resistance. Finally, ring current is determined as 2141.8 A.

The rotor bar parameters can be calculated in this step. The rotor shape of the task motor shown in Figure 1 is previously known from the company catalogue as it is, double caged. However, if the researcher has no idea about construction, then it would be a complex statistical analysis to find an appropriate solution regarding lots of possible types or NEMA standards can be another option to make an assumption. There is no way to understand the type of cage by physical detection except assumption that large frame motors can be double caged. The definite shape of the rotor bar is the center of the analysis in this proposed method. Moreover, it should be kept in mind that the rotor is the most important part of a machine; a small change in each parameter can affect all motor performance. On the other hand, it should be known that any change in each parameter will affect leakage reactance positively or negatively. Increase in leakage reactance will reduce the starting torque. According to these facts, the fitness function of the rotor bar used in heuristic parameter estimation, of which a representative picture is given in Figure 1, is obtained through the equation given by

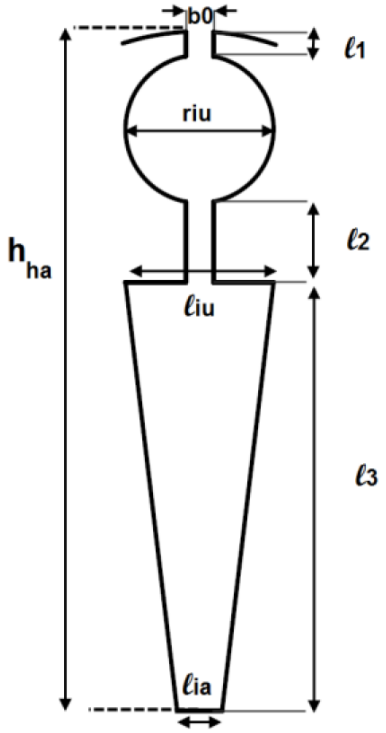

Figure 1. Diagram of rotor bar.

$$q_{ck} = (l_1 + l_2)\, b_0 + \pi r_{iu}^2 + \frac{2.r_{iu} + l_{ia}}{2}.(h_{ha} - (l_1 + l_2 + 2.r_{iu})) \tag{9}$$

Here q_{ck} and h_{ha} represent rotor bar cross sectional area and ring height, respectively. All parameters in Eq. (4) should be considered on mm basis.

2.1. Determination of electrical and geometrical boundary conditions for rotor bars

Electrical boundary conditions for rotor bars include the following conditions:

- Because of the cooling problems of high power machines, rotor bar current density must not be higher than 3 A/mm^2. Therefore, the limits of current density are from 1.5 to 3 A/mm^2. Thus the rotor bar resistance is calculated as follows:

$$R_{ck} = \frac{\rho_{al}.L\,.\,s_{ck}}{I_{ck}}\ (\Omega) \tag{10}$$

Here R_{ck}, ρ_{al}, L, and s_{ck} represent rotor bar resistance, aluminum specific resistance, rotor lamination sheet packet length (m), and rotor conductor current density (A/mm^2), respectively.

- Again because of the cooling problems of high power machines, rotor teeth induction density must not be higher than 1.5 T. Thus, in order to estimate the rotor teeth width by using the arc-dimension value shown in Figure 2, rotor teeth width depending on N_2 rotor slot number can be approximately as in Eqs. (6) and (7),

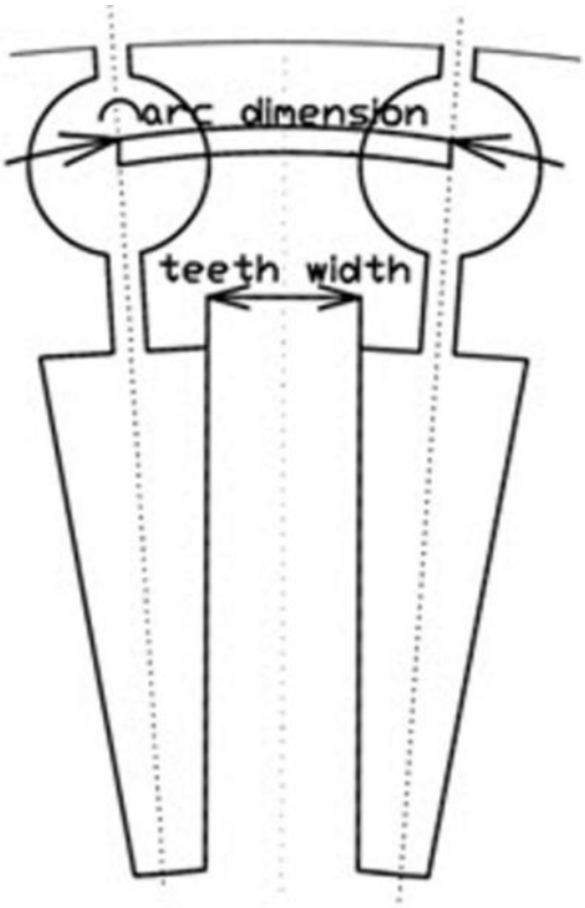

Figure 2. Basic parameters in estimation of rotor teeth width.

$$b_{d2} = (arc - dimension) - r_{iu}\ (m) \tag{11}$$

$$arc-dimension = \frac{\pi.(D_i - 2.\delta_0}{N_2} - b_0\ (m) \tag{12}$$

In Eqs. (6) and (7), b_{d2}, D_i, δ_0, b_0, and r_{iu} represent rotor teeth width, stator inner diameter, air gap, rotor slot mouth width, and outer cage conductor diameter, respectively.

Since all the parameters in Eq. (7) are directly measured from the task machine, the only unknown parameter r_{iu} and consequently rotor teeth width can be determined based on the following conditions:

The arc-dimension in Figure 2 is 20.37 mm for this machine. Therefore, the outer cage rotor bar diameter cannot be longer than about 10 mm, which is half of this value approximately, because the rotor teeth flux density increases up to more than 1.5 T, which is unacceptable for high power machines as mentioned in section 2.1.

- On the other hand, according to the max power theorem that slot teeth width and slot width must be equal to each other, the radius of outer cage cannot be less than 5 mm. However, this rule may go wrong in some cases in favor of slot teeth, and sometimes against it.

- Due to some leakage reactance calculations, inner cage trapezoid bottom length, l_{ia}, cannot be less than 0.1 mm and higher than half of l_{iu}.

After the estimation of b_{d2} depending on the aforementioned criteria, possible rotor teeth flux density values can be obtained by using air gap flux density value (B_0) determined in the stator calculations as follows:

$$B_{d2} = \frac{\tau_{02}.B_0}{k_{fe}.b_{d2}}\ (T) \tag{13}$$

τ_{02} and k_{fe} represent rotor slot divisions and iron fill factor, respectively. On the other hand, B_{d2} must be between 1.2 and 1.5 T to agree with design limitations in high power machines.

Since even a change of 0.1 mm in each parameter of the rotor bar affects starting, break down, and rated torque values, the simulation results are to be perceived from this perspective. In double cage motors the other following issues should be noted:

- Outer cage always has a rounded conductor.

- If inner cage is trapezoid shaped, long side width of trapezoid equals the outer cage conductor diameter.

- Rotor slot mouth width equals the conductor width of connection between outer and inner cage.

- l_1 distance should not be longer than l_2.

All measurement related to the ring can be performed externally. The ring width and height for this machine were, respectively, 17.38 mm and 57 mm. Using these measurements, ring section and current density can be calculated easily. Consequently, rotor resistance can be calculated by the equation given below [28],

$$R_2 = R_{ck} + \rho_{al}\,.\,\frac{D_{ha}\,(m)\,.\,N_2}{2.p^2.\pi.q_{ha}}\ (\Omega) \tag{14}$$

Here D_{ha} is the average of the inner and outer diameter of the ring and q_{ha} is the ring section area. Since stator yoke height can be calculated from Table 2, flux density of the yoke is

$$h_{j1} = \frac{\frac{\emptyset}{2}}{L_i . B_{j1}} \tag{15}$$

B_{j1} stator yoke flux density is determined as 1.6 T. Then after calculation of the Carter factor the magnetization current and saturation factor expression is

$$I_m = \frac{mmf_{tot}.p}{0.9.m_1.w_1.k_w} \ (A) \tag{16}$$

Here mmf_{total} is the total magneto motor force and it is

$$mmf_{total} = mmf_{\delta} + mmf_{d1} + mmf_{d2} + mmf_{j1} + mmf_{j2} \tag{17}$$

δ, d, and j are air gap, teeth, and yoke, respectively. Subscripts of 1 and 2 define stator and rotor. The saturation factor

$$k_{d0} = \frac{mmf_{total}}{mmf_{\delta}} \tag{18}$$

is a significant parameter in induction machine design and it must not be more than 2. The leakage inductance of stator and rotor are

$$X_{10} = 0.5.10^{-8}\pi^2 \frac{f}{p} .w_1^2 . (\lambda_{01} + \lambda_{b1} + \lambda_{ha1}) \ \Omega/\text{phase} \tag{19}$$

and

$$X_{20} = 0.85.10^{-8}\pi^2 f .w_1^2 . (\lambda_{02} + \lambda_{b2} + \lambda_{ha2}) \ \Omega/\text{phase} \tag{20}$$

respectively. λ_0, λ_b, and λ_{ha} are the magnetic distribution conductivity of active winding, front winding, and ring. Subscripts 1 and 2 show stator and rotor. After finding these values nominal and starting torque can be calculated by the well-known torque formula using equivalent circuit parameters.

3. Improved PSO

Since PSO is relatively simple algorithm and converges quickly it is applied widely to numerical problems that require high CPU time. However, PSO cannot find the exact solution all the time and so hybrid PSO algorithms are presented. On the other hand, reduction of CPU time is highly recommended in complex architectures, which is the goal of this improvement. The flowchart of the improvement based on initialization of particles is shown in Figure 3. Weighted selection is preferred to reduce the swarm size. The population size is reduced to half of its initial value in terms of minima or maxima problem. Thus the CPU time is significantly reduced in the main loop of the algorithm. Test and analysis results of improved PSO and comparison with conventional PSO are indicated in Table 3. All simulations have been run a thousand times for the same initial population and convergence value and average values are included.

The De Jong 1 function is one of the simplest test functions. It has a continuous and convex format. The global optimum value in the De Jong 1 function is zero and is independent of the number of variables. Same and significant reduction in terms of CPU time has been obtained. The De Jong 2 function is a classic optimization function, and at the same time it is known as a "banana function" or the Rosenbrock's function. The global

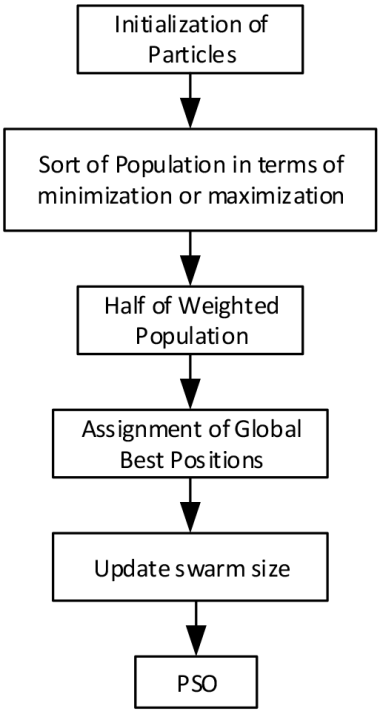

Figure 3. Flowchart of improved PSO.

Table 3. CPU time analysis for improved PSO and results.

Test functions	Number of variables	Mathematical expression	PSO		Improved PSO		Reduction in CPU time (%)
			Iterations	CPU time (s)	Iterations	CPU time (s)	
DeJong1	3	$f(x) = \sum_{i=1}^{n} x_i^2$	80.1	35.99	59.308	15.23	0.58
	10		168.8	75.64	128.4	31.52	0.58
DeJong2	3	$f(x) = \sum_{i=1}^{n-1} 100 \cdot \left(x_{i+1} - x_i^2\right)^2 + (1 - x_i)^2$	62.248	9.138	45.6	5.71	0.38
	10		123.4	28.6	113.2	16.652	0.42
DeJong3	3	$f(x) = \sum_{i=1}^{n} int(x_i)$	116.4	35.44	79.42	28.28	0.20
	10		107.25	106	98.25	55.25	0.48
DeJong4	3	$f(x) = \sum_{i=1}^{n} ix_i^4 + Gauss(0,1)$	19,011	8276	488.6	4512	0.45
	10		21,237.6	10,411.6	548.4	8452	0.19
DeJong5	3	$f(x) = \sum_{i=1}^{m} \frac{1}{\sum_{j=1}^{4} \left(x_j - a_{ij}\right)^2 + c_i}$	63.4	89.12	43.688	33.78	0.62
	10		111.92	511.25	200.9	461.75	0.10
Rastrigin	3	$f(x) = 10n + \sum_{i=1}^{n} \left(x_i^2 - 10\cos(2\pi x_i)\right)$	112.12	133.5	114.125	79.7	0.40
	10		178.3	605.83	170	294.4	0.51

optimum point is in a deep parabolic shaped valley; its value is zero and is independent of the number of variables. Because it is hard to find the minimum point in the valley, this function is used for performance tests. Similar improvements are observed as De Jong1. The De Jong 3 function is a step, discontinuous, unimodal,

separable, and scalable function. The global optimum value in the De Jong 3 function depends on the number of variables. A 20% reduction has already obtained for three variables while it is 48% for ten, which is good news for improved PSO. The De Jong 4 function is a dimensional quartic function with Gaussian noise. An average value of about 20% is the result for more variables and 45% is noticeable for three variables. The De Jong 5 function is known as Shekel's function, and the quantities a_{ij} and c_i are given in Table 4. Shekel's function is a two-dimensional, continuous, multimodal, separable function with local maxima related to the a_{ij} matrix. It is interesting to see a good performance (62%) for three variables, but only 10% for ten. The Rastrigin function is obtained by modifying the De Jong 1 function by a cosine module. In this function, there are many local minima that are uniformly distributed. Closer and excellent reduction values are obtained. Finally improved PSO manifests itself in reduction of CPU time for all test functions significantly.

Table 4. Coefficients for Shekel's function (m = 7).

i	a_{ij} (j = 1 ... 4)				c_i
1	4	4	4	4	0.1
2	1	1	1	1	0.2
3	8	8	8	8	0.2
4	6	6	6	6	0.4
5	3	7	3	7	0.4
6	2	9	2	9	0.6
7	5	5	3	3	0.3

4. Application of simulations and results

The real parameter-based heuristic algorithms are used to find the optimal parameters of the rotor slot in this study. GA is a well-known evolution algorithm modeling the biologic procedure and optimizing functions. GA is capable of finding a global optimum without stopping at local points regarding the fitness function that characterizes the system response. GA may find a local optimum with these operators, not the real extremums. To overcome this disadvantage mutation is used. Easy implementation, less parameters in the algorithm, and fast convergence are the main advantages of PSO. PSO is a good option for systems requiring hard CPU times. PSO, improved PSO, and GA are also compared with each other in terms of CPU time.

The fitness function of the system is the total amount of nominal and starting torque, power factor, and efficiency as given in Eq. (21). These are known parameters of the current motor, which is the main reason for this parameter selection. Each individual represents a chromosome containing six bits for each parameter as shown in Eq. (22). The chromosome is the section area of the rotor slot, which was defined in Eq. (9). The applied procedure of GA simulation is summarized in the flowchart shown in Figure 3.

$$O(X) = T_n + T_s + PF + Eff \tag{21}$$

$$X = [l_1\, l_2\, r_{iu}\, l_{ia}] \tag{22}$$

where T_n, T_s, PF, and Eff are rated and starting torque, power factor, and efficiency, respectively. In Eq. (21) the expansion of each component is

$$O(X) = \left|\frac{T_{nsim}}{1029} - 1\right| + \left|\frac{T_{ssim}}{2470} - 1\right| + \left|\frac{PF_{sim}}{0.87} - 1\right| + \left|\frac{Eff_{sim}}{0.95} - 1\right| \tag{23}$$

This gives the total error regarding motor test values in Table 1 that are fixed as constants. Subscript sim defines calculated values by the heuristic simulation. The simulation included FEM runs to find optimal values corresponding to minimum error as shown in the flowchart in Figure 4.

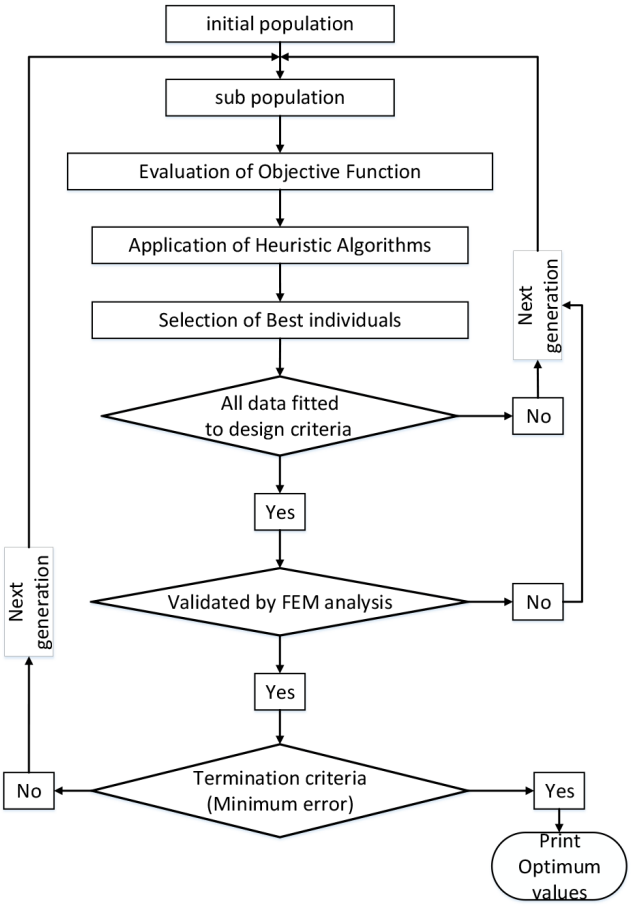

Figure 4. Flowchart of optimization of heuristic algorithms with FEM application.

Through the criteria given in the theoretical approach in section 2, the parameters and the boundaries for the heuristic simulations can be considered as l_1, l_2, r_{iu}, and l_{ia}, which are the geometric parameters of the rotor bar given in Eq. (4). The first step is to create the data pool r_{iu} values corresponding to rotor teeth flux density limitations stated in section 2.1 by using Eq. (7) for the selection process in heuristic simulation to avoid possible inconsistent results. The second step is to create a population. Then the rest of the simulation runs in the usual way. Some basic experimental results of the 160 kW machine and the results obtained by heuristic algorithms are given in Table 5. Heuristic simulation parameters and results, boundary conditions, and real values are given in Table 6. Improved PSO is named PSO2 in these tables. The rest of the parameters are summarized in Table 7. Comparison of the three algorithms in terms of CPU time is displayed in Table 8.

The results obtained through heuristic algorithms are very close to the real values in Table 5. Moreover, all simulation results are around the experimental results in Table 6. The last three rows in that table have no boundary conditions because they are dependent parameters. While the results in this table are nice, it is still a fact that this is a misleading result in Table 6 for researchers, because when the bar parameters in Table 6 are analyzed precisely the following issues will be noted for the three simulations:

Table 5. Simulation results and real values of 160 kW induction machine.

Parameter definition	PSO PSO2 GA	Real	Fault ratio (%)
Nominal torque (Nm)	1028,9	1029	≈ 0
Starting torque (Nm)	2481	2469	0.48
Revolutions per minute	1490	1485	0.336
Power factor	0.88	0.87	1.1
Copper loss (kW)	6.4	6.5	1.5
Iron+friction loss (kW)	5	5.1	0.4
Efficiency (%)	93.3	95	1.79
Total			3.7

Table 6. Rotor bar boundaries for PSO, PSO2, GA, simulation results, and real values.

Rotor slot parameters (mm)	Definition	Lower bound	Upper bound	PSO	PSO2	GA	Real
ℓ_1	The height between outer surface of the rotor and outer cage	0.25	0.9	0.68	0.59	0.64	0.5
ℓ_2	The height between outer cage and inner cage	2	8	5.8	5.87	5.6	5
r_{iu}	Outer cage conductor diameter	6	10	9.66	9.66	9.46	8
ℓ_{ia}	Inner cage conductor bottom length	1	r_{iu}	1	1	1	3.03
h_{a2}	Lower cage conductor height			40.86	40.88	41.3	36.5
h_{02}	Total conductor height			57	57	57	53
R_2	Rotor Resistance ($10^{-5}\Omega$)			8.006	8.008	7.9969	7.9925

Table 7. Simulation results for other motor parameters.

Symbol	Definition	Unit	GA	PSO	PSO2
I_n	Rated current	A	284 284 284		
I_m	Magnetizing current	A	72	71.5	71.5
I_{ha}	Ring current	A	2141 2141		
I_{21}	Equivalent rotor current refer to primary side	A	147 147		
φ	Total flux	Wb	0.057	0.055	0.055
E_1	EMK at the stator winding	V	376.2 376.2		
R_1	Stator winding resistance	Ω	0.022 0.022		
R_{21}	Equivalent rotor resistance refer to primary side	Ω	0.02 0.02		
R_2	Real rotor resistance (10^{-5})	Ω	7.996	8.006	8.008
B_{j1}	Stator yoke flux density	T	1.47 1.47		
B_{j2}	Rotor yoke flux density	T	1.6 1.6		
k_c	Carter factor		1.17	1.175	1.175
k_{d0}	Saturation factor		1.66	1.64	1.64
X_m	Magnetizing reactance	Ω	2.5		
X_{10}	Stator winding leakage reactance	Ω	0.0522 0.0522		
X_{20}	Rotor winding leakage reactance referred to primary	Ω	0.485	0.486	0.486
s	Slip		0.0065		

- A very small increase occurred in l_1. However, the result and the reflection of this small increase would not be at the same ratio, and this causes the distance between the entire cage and shaft to be increased and output moment to be decreased.

Table 8. Comparison of algorithms in terms of CPU time.

Algorithm	CPU time
PSO	1.35 s
PSO2	0.51 s
GA	0.13 s

- Still a very small difference in l_2 will mean that the inner cage will be slightly more embedded inward and it will cause leakage fluxes to be slightly greater. This means that the starting torque value will change improperly in particular.
- An increase in r_{iu} will cause copper losses to be reduced, but rotor flux density will be in trouble proportionally. This difference is more acceptable than the effect of the two aforementioned parameters.
- Since total rotor conductor is assumed equal to ring height in the simulation, the difference in l_{ia} value will affect total rotor section directly, and so it has a great importance and similarly it will also affect all torque values directly. It also is expected that r_{iu} will be bigger than the real value because the optimum l_{ia} value of iteration for the simulations is 1 mm and r_{iu} has to be bigger than the real value to eliminate the decrease in the trapezoid inner cage conductor.
- On the other hand, l_{ia} value is 1 mm in the three simulations while the real one is 3 mm. This can also be a contradiction, but since the r_{iu} dependency limits this parameter it is an expected value because of algorithm topology, which is focused on r_{iu} to fix the cross section area of the rotor conductor.
- Rotor resistance value shows the total section area of the rotor conductor is absolutely correct.

Regarding total conductor heights, as an initial condition for simulation, the height of the ring was assumed equal to the height of the rotor conductor, whereas the real height of the ring is bigger than the total height of the conductor. This is obviously done like that so as to adjust the rotor resistance. Almost the same results are obtained through these two cases in terms of determination of rotor resistance. As a result of that, in the simulations, since total height of the conductor was assumed equal to the height of the ring, the section of the inner cage was reduced so as to make rotor resistance equal. It can be concluded from Table 6 that although the real results do not match the simulation ones for the rotor bar parameters, the main outputs of the motor are obtained very precisely. In addition, it should be known that the usual researcher must have an idea about the usual shape of the rotor slot of the task machine that will be studied, because it may be impossible to find a solution especially for double caged motors that have a wide variety of rotor slot types. In Tables 5 and 6 in the calculations made based on electrical machine design, an error between 10% and 20% is tolerable. Owing to nonlinearity and unexpected behavior of the induction machine, this toleration band is acceptable in electric machine designs. Accordingly, the error ratio in Table 5 is almost perfect. It should be kept in mind again that although the changes in the first four rotor bar parameters are small on a mm basis, due to the rotor being the "heart" of the motor even small changes will have a great effect on moment and efficiency values. Therefore, while simulation results are misleading, they should be used for the purpose of giving an idea.

The CPU times for PSO, improved PSO (PSO2), and GA are indicated in Table 8. While all algorithms find similar optimum values they have different CPU times. Firstly, a significant improvement is reduction in CPU times as it is expected in PSO2 obtained as more than 50%. Thus selection of improved PSO for complex systems will reduce CPU time drastically. While GA has shorter simulation time in this system, it can be the best choice for noncomplex structures.

The results of FEM analysis including induction density and flux lines of the machines simulated with real values and heuristic simulation are given in Figures 5–8, respectively. Flux density yielded close to the designed values for the two cases. On the other hand, a very obvious difference was unexpected in both designs, and that was just what happened. However, the same result will not be obtained in the experimental test due to the reasons mentioned above.

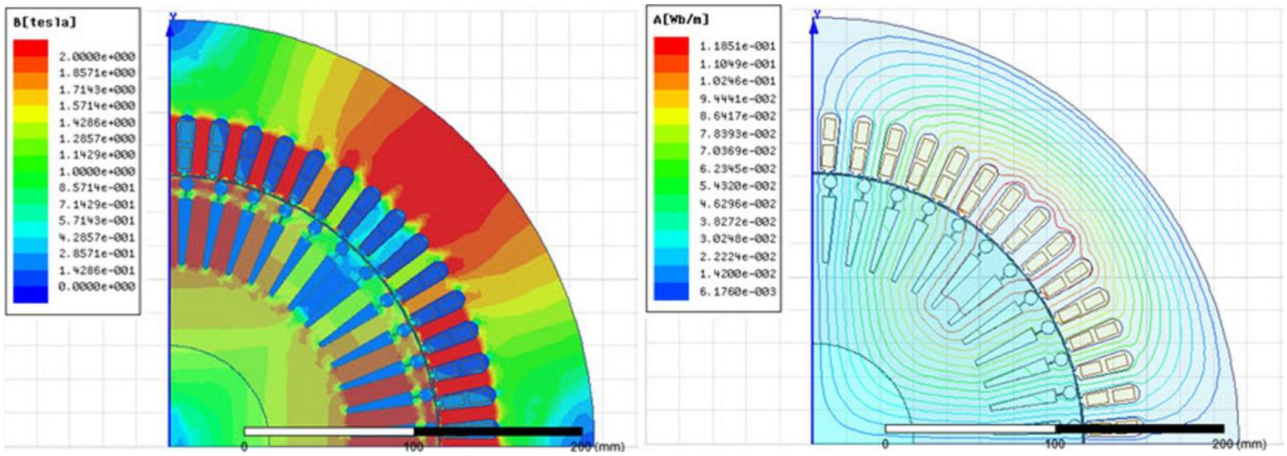

Figure 5. Finite element results for real machine.

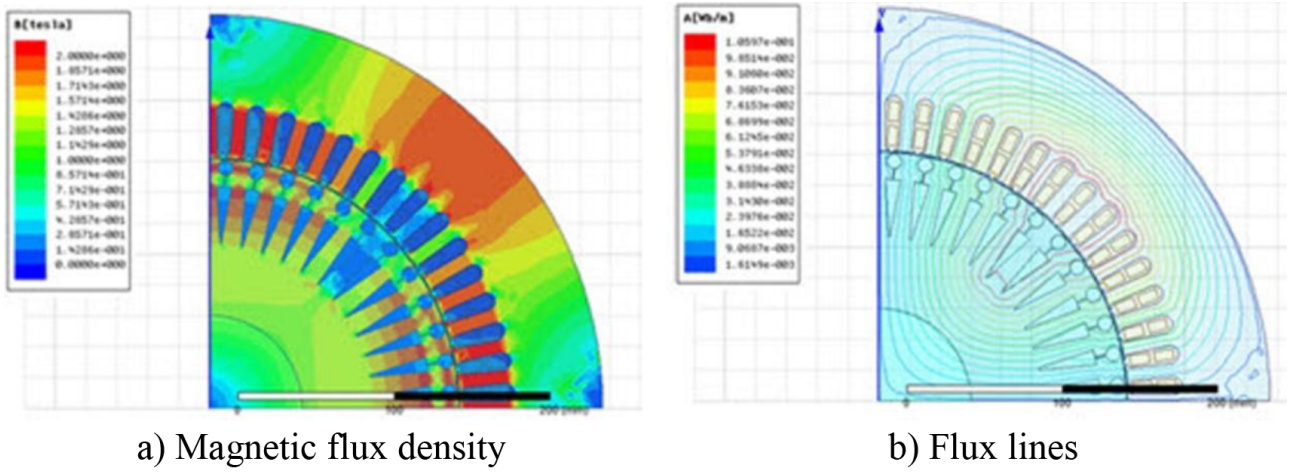

Figure 6. Finite element results for GA simulated machine.

The first noticeable issue is in detailed analysis due to rotor slot bottoms being broader in the design of heuristic algorithms flux density decreased naturally. Secondly, due to the distance between the outer cage and the inner cage being more in heuristic simulation flux density at the rotor core decreased. On the other hand, the stator core flux density of heuristic simulation decreased apparently. Although flux lines are different from each other in reality, they are not apparent. Finally it can be concluded that heuristic simulation has better flux density results in total compared with the real one.

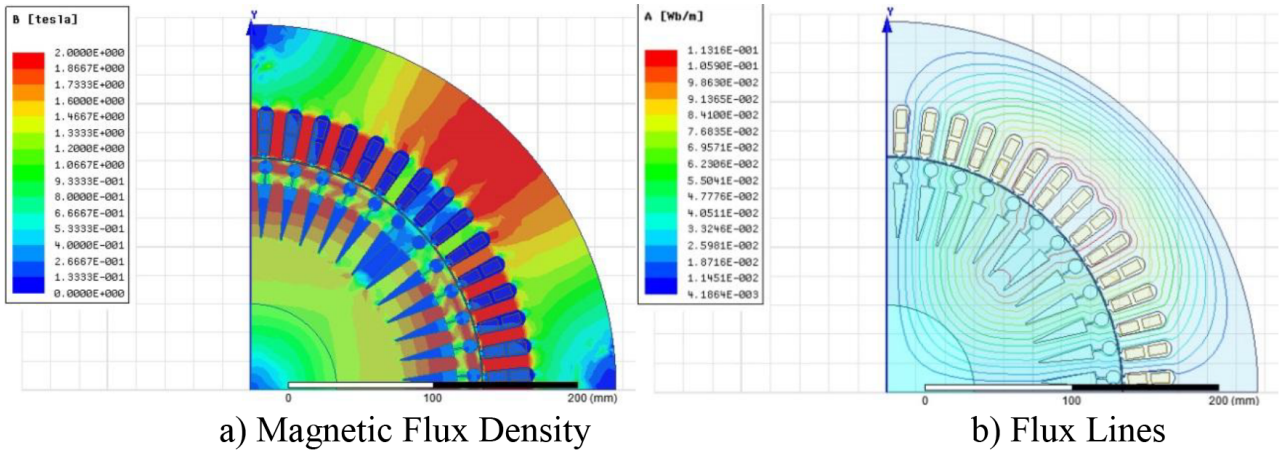

Figure 7. Finite element results for PSO simulated machine.

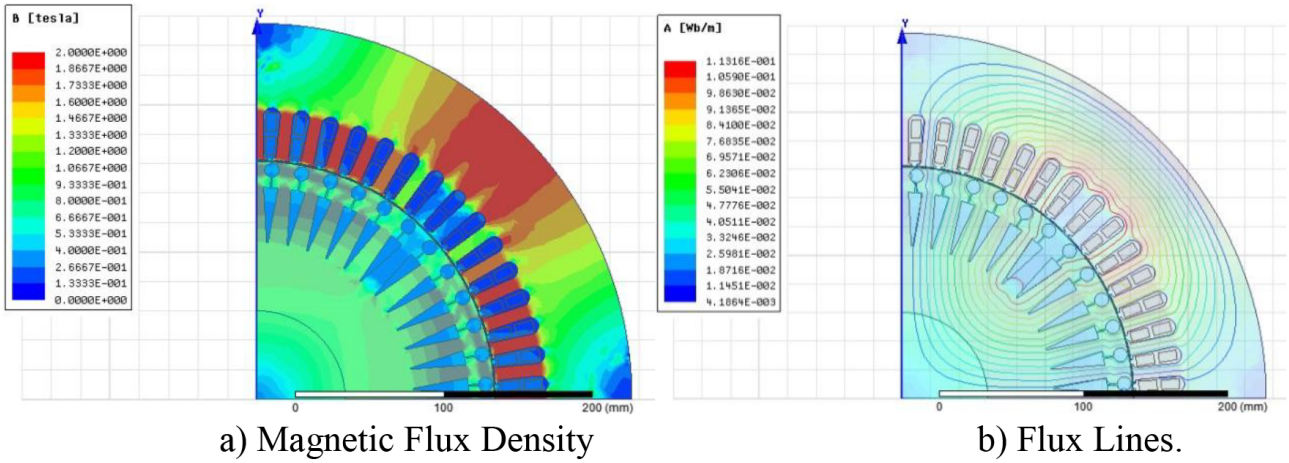

Figure 8. Finite element results for PSO2 simulated machine.

5. Conclusion

In recent years, the determination of induction machine equivalent circuit parameters accurately is important in terms of electrical calculations and machine characteristics. While the stator ones could be measured externally easily, the rotor is a closed box and so rotor slot shape and dimensions could not be determined externally. For the cases when the rotor lamination drawing could not be obtained or breaking the rotor pieces is not possible and also not desired, a methodological analysis is presented in order to determine the rotor slot parameters in this study. Heuristic simulation results validated by FEM and the experimental ones were compared and the following conclusions are drawn:

- Through heuristic simulations, the motor's main output parameters can be determined almost precisely.
- Although rotor slot parameter values of the simulation are close to the real ones on mm basis, it should be taken into consideration that even small changes in the rotor part will have a great effect on the mechanical power of the motor.
- Magnetostatic analysis results regarding saturation effect and flux density are close to each other, but heuristic simulations have better max flux density values at the center of each pole at the stator and at the bottom of slots for the rotor.

A significant improvement in the reduction of CPU times is obtained for improved PSO of more than 50%. Thus selection of improved PSO for complex systems will reduce CPU time drastically. On the other hand, comparison of CPU time with GA shows conventional PSO is a not a good option for optimization of noncomplex architectures. While GA has shorter simulation time in this system, it can be the best choice for noncomplex structures; the second option can be improved PSO for mid-complex systems. A high power machine is used as a test machine in this study concerning the matters described in Section 1. The proposed method will also work with low power induction machines.

References

[1] Was M, Krzeminski Z, Toryat HA. Neural-network-based parameter estimations of induction motors. IEEE T Ind Electron 2008; 55: 1783-1794.

[2] Maitre J, Gaboury S, Bouchard B, Bouzouane A. An effective identification of the induction machine parameters using a classic genetic algorithm, NSGAII and θ-NSGA III. In: 2015 6th International Conference on Information, Intelligence, Systems and Applications; 2015. pp. 1-6.

[3] Kampisios K, Zanchetta P, Geraga C, Trentin A, Jasim O. Induction motor parameters identification using genetic algorithm for varying flux levels. In: 2008 13th Power Electrinics and Motion Control Conference, 2008. pp. 887-892.

[4] Kwon C, Sudhoff D. Genetic algorithm-based induction machine characterization procedure with application to maximum torgue per amp control. IEEE T Energy Conv 2006; 21: 405-415.

[5] Raie A, Rastchi V. Accurate identification of parameters, in winding function model of induction motor, using genetic algorthm. In:2002 Proceedings of the 41st SICE Annual Conference, 2002. pp. 2430-2434.

[6] Huynh DC, Dunnigan MW. Parameter estimation of an induction machine using advanced particle swarm optimization algorithms. IET Elec Power Appl 2010; 4: 748-760.

[7] Huynh DC, Dunnigan MW. Parameter estimation of an induction machine using a dynamic particle swarm optimization algorithms. In: 2010 IEEE International Symposium on Industrial Electronics, 2010. pp. 1414-1419.

[8] Huynh DC, Dunnigan MW. Parameter estimation of an induction machine using a chaos particle swarm optimisation algorithms. In: 2010 5th IET International Conference on Power Electronics, Machines and Drives, 2010. pp. 1-6.

[9] Ojaghi M, Daliri S. A detailed dynamic model for single-phase shaded pole induction motors. In: 2015 18th International Conference on Electrical Machines and Systems, 2015. pp. 1987-1992.

[10] Riveros JA, Reina DG, Barrero F, Toral SL, Duran MJ. Five-phase induction machine parameter identification using PSO and standstill techniques. In: 2015 Industrial Electronics Society, 41st Annual Conference of the IEEE, 2015. pp. 613-618.

[11] Grewal GS, Rajpurohit BS. Induction machine efficiency estimation using population based algorithm. In: 2014 IEEE 6th India International Conference on Power Electronics, 2014. pp. 1-6.

[12] Yousfi L, Bouchemha A, Bechouat M, Boukrouche A. Induction machine parameter identification: a comparison between GAs and PSO approaches. In: 2013 8th International Conference and Exhibition on Ecological Vehicles and Renewable Energies; 2013. pp. 1-5.

[13] Tofighi EM, Mahdizadeh A, Feyzi MR. Online estimation of induction motor parameters using a modified particle swarm optimization technique. In: 2013 Industrial Electronics Society, 39th Annual Conference, 2013. pp. 3645-3650.

[14] Ramya AS, Raja P. Estimation and performance evalution of an induction machine using optimization techniques. In: 2012 IEEE International Conference on Power Electronics, Drives and Energy Systems, 2012. pp. 1-6.

[15] Telford D, Dunnigan MW, Williams BW. Online identification of induction machine electrical parameters for vector control loop tuning. IEEE T Ind Electron 2003; 50: 253-261.

[16] Huang KS, Wu QH, Turner DR. Effective identification of induction motor parameters based on fewer measurements. IEEE T Energy Conv 2002; 17: 55-60.

[17] Faiz J, Sharifian MBB. Different techniques for real time estimation of an induction motor rotor resistance in sensorless direct torque control for electric vehicle. IEEE T Energy Conv 2001; 16: 104-109.

[18] Duan F, Zivanovic R, Al-savari S, Mba D. Induction motor parameter estimation using sparse grid optimization algorithm. IEEE T Ind Info 2016. pp. 1-1.

[19] Uphues A, Nötzold K, Wegener R, Soter S. Comparison of parameter identification approaches with linearised process models based on PLS for induction machine with P > 100kW. In: 2016 IEEE International Conference on Industrial Technology, 2016. pp. 134-140.

[20] Tekgun B, Sozer Y, Tsukerman I. Modeling and parameter estimation of split-phase induction motors. IEEE T Ind Appl 2016; 52: 1431-1440.

[21] Lee SB, Habetler TG, Harley RG, Gritter DJ. A stator and rotor resistance estimation technique for conductor temperature monitoring. IEEE Ind Appl 2000; 1: 381-387.

[22] Boglietti A, Cavagnino A, Lazzari M. Computational algorithms for induction-motor equivalent circuit parameter determination-part I: resistances and leakage reactances. IEEE T Ind Electron 2011; 58: 3723-3733.

[23] Boglietti A, Cavagnino A, Lazzari M. Computational algorithms for induction motor equivalent circuit parameter determination-part II: skin effect and magnetizing characteristics. IEEE T Ind Electron 2011; 58: 3734-3740.

[24] Lee SJ, Kim JM, An DK, Hong JP. Equivalent circuit considering the harmonics of core loss in the squirrel-cage induction motor for electrical power steering application. IEEE T Magn 2014; 50.

[25] Pedra J, Sainz L. Parameter estimation of squirrel-cage induction motors without torque measurements. Iee Proce-Elec Power Appl 2006; 153: 263-270.

[26] Zhou P, Gilmore J, Badics Z, Cendes ZJ. Finite element analysis of induction motors based on computing detailed equivalent circuit parameters. IEEE T Magn 1998; 34: 3499-3502.

[27] Lin WM, Su TJ, Wu RC. Parameter identification of induction machine with a starting no-load low-voltage test. IEEE T Ind Electron 2012; 59: 352-360.

[28] Campos-Delgado DU, Arce-Santana ER, Espinoza-Trejo DR. Edge optimisation for parameter identification of induction motors. IET Elec Power Appl 2011; 5: 668-675.

[29] Repo AK, Rasilo P, Arkkio A. Dynamic electromagnetic torque model and parameter estimation for a deep-bar induction machine. IET Elec Power Appl 2008; 2: 183-192.

[30] Castaldi P, Tilli A. Parameter estimation of induction motor at standstill with magnetic flux monitoring. IEEE T Contr Syst T 2005; 13: 386-400.

[31] Derdiyok A. Simple method for speed and rotor resistance estimation of induction machines. IEE Proce-Elec Power Appl 2003; 150: 289-294.

[32] Boduroğlu, T. The Lessons of Electric Machinery, Transformers. İstanbul, Turkey: Beta, 1988.